International Journal of Pharmaceutics: X 5 (2023) 100183

Contents lists available at ScienceDirect

International Journal of Pharmaceutics: X

journal homepage: www.sciencedirect.com/journal/international-journal-of-pharmaceutics-x

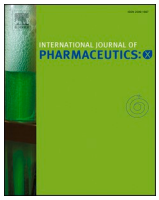

Efficient ocular delivery of siRNA *via* pH-sensitive vehicles for corneal neovascularization inhibition

Xiaowen Cao [a,1], Changrong Wang [b,1], Zhennv Deng [a], Yiming Zhong [a], Hao Chen [a,*]

[a] School of Ophthalmology and Optometry/School of Biomedical Engineering, Eye Hospital, Wenzhou Medical University, Wenzhou, Zhejiang 325027, China
[b] Engineering Research Center of Molecular & Neuroimaging, Ministry of Education, School of Life Science and Technology, Xidian University, Xi'an, Shaanxi 710126, China

ARTICLE INFO

Keywords:
Cornea neovascularization
Anti-angiogenesis
siRNA delivery
pH-sensitive polymer

ABSTRACT

Corneal neovascularization (CoNV)-induced blindness is an enduring and challenging condition with limited management options. Small interfering RNA (siRNA) is a promising strategy for preventing CoNV. This study reported a new strategy using siVEGFA to silence vascular endothelial growth factor A (VEGFA) for CoNV treatment. To improve the efficacy of siVEGFA delivery, a pH-sensitive polycationic $mPEG_{2k}$-$PAMA_{30}$-P(DEA_{29}-$D5A_{29}$) (TPPA) was fabricated. TPPA/siVEGFA polyplexes enter cells *via* clathrin-mediated endocytosis, resulting in higher cellular uptake efficiency and comparable silencing efficiency than that of Lipofectamine 2000 *in vitro*. Hemolytic assays verified that TPPA safe in normal physiological environments (pH 7.4) but can easily destroy membranes in acidic mature endosomes (pH 4.0). Studies on the distribution of TPPA *in vivo* showed that it could prolong the retention time of siVEGFA and promote its penetration in the cornea. In a mouse model induced by alkali burn, TPPA efficiently delivered siVEGFA to the lesion site and achieved VEGFA silencing efficiency. Importantly, the inhibitory effect of TPPA/siVEGFA on CoNV was comparable to that of the anti-VEGF drug ranibizumab. Delivering siRNA using pH-sensitive polycations to the ocular environment provides a new strategy to efficiently inhibit CoNV.

1. Introduction

To ensure clarity and optimal vision, the cornea, a clear tissue in the front of the eye, must be avascular. Many conditions, such as excessive contact lens wearing, corneal infection, and injury can lead to corneal neovascularization (CoNV), resulting in corneal opacity, vision loss, and blindness (Arbabi et al., 2019; Wang et al., 2017). CoNV is one of the most common causes of blindness worldwide, affecting >1.4 million people annually in the United States alone (Lee et al., 1998). Therefore, inhibiting the formation of CoNV is important for maintaining a normal ocular surface. Traditionally, there are two therapeutic approaches for treating CoNV: medicine and surgery (Feizi et al., 2017; Roshandel et al., 2018). For medical treatment, long-term medication carries a potential risk of cataract, glaucoma, and superinfection (Gupta and Illingworth, 2011), whereas the efficacy of surgical treatments mainly dependents on the operator's technique (Chu et al., 2020). Thus, there is an urgent need to develop an efficient and safe method for inhibiting CoNV.

Small interfering RNA (siRNA), which can degrade messenger RNA (mRNA) or downregulate specific genes through the RNAi pathway, has attracted much attention for the treatment of various diseases (Baran-Rachwalska et al., 2020; Wang et al., 2017). Gene therapy has recently been introduced to treat corneal diseases (Baran-Rachwalska et al., 2020; Fernando et al., 2018; Wels et al., 2021). Although the efficacy of gene therapy for corneal diseases has improved, defects in the gene itself and the inherent physical barriers in the eyeball remain great challenges for gene delivery (Wang et al., 2017; Wels et al., 2021). As a small nucleic acid molecule, siRNA is negatively charged, limiting its penetration through cell membranes (Truong et al., 2013). Moreover, naked siRNA is fragile and easily degraded by widely available nucleases (Semple et al., 2010). The main intrinsic physical barriers of the cornea,

Abbreviations: TEM, Transmission electron microscopy; DLS, dynamic light scattering; CLSM, Confocal laser scanning microscopy; FACS, Fluorescence-activated cell sorting; GPC, Gel permeation chromatography; HCECs, Human corneal epithelial cells; HUVECs, Human umbilical vein endothelial cells; MFI, Mean fluorescence intensity.

* Corresponding author.
E-mail address: chenhao@mail.eye.ac.cn (H. Chen).
[1] These authors contributed equally to this work

https://doi.org/10.1016/j.ijpx.2023.100183
Received 15 February 2023; Received in revised form 5 April 2023; Accepted 28 April 2023
Available online 29 April 2023

tear film, mucin layer, epithelium, Bowman's layer, stroma, Descemet's membrane, and the endothelium, protect the cornea but also pose great challenges for drug delivery(Wels et al., 2021). Therefore, it is necessary to overcome the problems of siRNA itself and the inherent obstacles of the cornea to improve the delivery efficacy of corneal siRNA.

To improve siRNA delivery efficiency, viral and non-viral vehicles have been designed. However, the biosafety of viral vectors remains a great limitation (Yin et al., 2014). Non-viral vehicles have the advantages of low cost, high plasticity, and low immunogenicity (Li et al., 2021; Upadhya et al., 2020; Wilson and Doudna, 2013). Among the non-viral vehicles, pH-sensitive polymers have been extensively studied. Studies have shown that improved gene delivery efficiency can be achieved by introducing pH-responsive fragments into gene delivery vectors (Asayama et al., 2008; Chandrashekhar et al., 2013; Chen et al., 2012; Kim et al., 2002; Park et al., 2020; Wilson and Doudna, 2013; Xu and Lu, 2011). Our previous study found that pH-sensitive polymers with pK_a values of 5.8–6.2 illustrated the best siRNA knockdown efficiency both *in vitro* and *in vivo* (Du et al., 2018). The A-B-C (A: amphiphilic sections, B: polycationic sections, C: pH-sensitive sections) triblock polycationic form was efficient for siRNA delivery (Wang et al., 2017). In addition, the gene knockdown efficacy of mPEG-$PAMA_{50}$-P(DEA_{39}-$D5A_{37}$) was increased up to 87.2% (Wang et al., 2021). Therefore, it is feasible to design pH-sensitive siRNA delivery vehicles.

To address the aforementioned issues of CoNV, we herein report a siVEGFA delivery strategy that combines our advantages with a pH-sensitive vehicle design to silence vascular endothelial growth factor A (VEGFA). Considering the high gene knockdown efficiency of mPEG-$PAMA_{50}$-P(DEA_{39}-$D5A_{37}$), we continued to use this structure and designed $mPEG_{2k}$-$PAMA_{30}$-P(DEA_{29}-$D5A_{29}$) (TPPA) as the delivery vehicle for siVEGFA. The TPPA NPs were able to bind to siRNA efficiently at *w*/w = 10/1. The VEGFA silencing efficiency was comparable to the common transfection reagent Lipo 2000 *in vitro,* attributed to its high cell endocytosis efficiency. The cytotoxicity assay verified that there was no significant cytotoxicity of TPPA/siRNA, even at w/w ratios up to 30/1. TPPA efficiently delivered siVEGFA to corneal cells and achieved VEGFA-silencing efficiency *in vivo*. The inhibitory effect of TPPA/siVEGFA on CoNV was comparable to that of the anti-VEGF drug ranibizumab.

2. Materials and methods

2.1. Materials

Chemical reagents such as 2-(diehtyl amino) ethyl methacrylate (DPA), MTT, $mPEG_{2k}$, chloroquine, and TRIzol were procured from Sigma Aldrich. Trypsin, fetal bovine serum, Dulbecco's modified Eagle's medium, Lipofectamine 2000, endocytosis inhibitors, and other biological reagents were provided by Sigma-Aldrich.

2.2. Synthesis of TPPA copolymer and polyplex preparation

First, AMA and D5A were prepared. Briefly, triethylamine and tert-butyl N-(2-hydroxyethyl) carbamate were first mixed in CH_2Cl_2, and then the methacrylate was added dropwise slowly at 0 °C. The reaction was carried out under Ar protection for 1 h, and then continued at room temperature for 12 h. The product was extracted, dried, and finally purified by recrystallization from CH_2Cl_2/hexane.

For the synthesis of D5A, first Na_2CO_3 and CH_3CN solutions were reacted at 80 °C overnight. The initial product was deprecipitated and distilled to obtain 2-(dipentylamino) ethanol. Then, 2-(dipentylamino) ethanol, triethylamine and methacryloyl chloride were dissolved in CH_2Cl_2 and reacted in a three-necked flask. Finally, the product was purified by filtration and distillation. The product structure was characterized by ^{1}H NMR (Varian Unity Plus INOVA 400).

The final product, $mPEG_{2k}$-*b*-PAMA-*b*-P(D5A/DEA), was synthesized by reversible addition-fragmentation chain transfer polymerization (RAFT). First, $mPEG_{2k}$-CTAm (0.2347 g, 0.1 mmol), AMA (0.8015 g, 3.5 mmol) and AIBN (3.28 mg, 0.02 mmol) were dissolved in 4 mL DMF. The mixture was then reacted under argon protection for 24 h at 70 °C, and the product $mPEG_{2k}$-PAMA (1.0120 g) was obtained after dialyzing and lyophilizing. Then $mPEG_{2k}$-PAMA (0.4609 g, 0.05 mmol), DEA (0.2775 g, 1.5 mmol), D5A (0.4035 g, 1.5 mmol) and AIBN (1.64 mg, 0.01 mmol) were dissolved in 4 mL DMF and reacted under argon protection at 70 °C for 24 h. After cooling to room temperature, the reaction mixtures were purified through dialysis and lyophilization to obtain the final product triblock polymer TPPA (1.1 g). The final product was characterized by ^{1}H NMR and GPC.

To prepare TPPA nanoparticles (NPs), TPPA was weighed, completely dissolved in trifluoroethanol overnight, added dropwise to PBS, and rotated at medium speed for 24 h, and then dialyzed in 100 kD for 2 h. TPPA was mixed with siRNA at different weight/weight ratios (*w*/w) and incubated at room temperature for 15 min to obtain TPPA/siRNA nanocomplexes. The siRNAs used in the experiments were obtained from Suzhou Ribo (China). The siNC sequence designed by RiBo was used as a negative control. The specific sequences (Kwak et al., 2017) were as follows:

siNC-sense strand, 5′-UUCUCCGAACGUGUCGUCACGUdTdT-3′
siNC-antisense strand, 5′-ACGUGACACGUUCGGAGAAdTdT-3′
Cy5-siNC-sense strand, 5′-Cy5-CCUUGAGGCAUACUUCAAAdTdT-3′
Cy5-siNC-antisense strand, 5′-UUUGAAGUAUGCCUCAAGGdTdT-3′
siVEGFA-sense strand, 5′-GGAGUACCCUGAUGAGAUdTdT-3′
siVEGFA-antisense strand, 5′-AUCUCAUCAGGGUACUCCdTdT-3′

2.3. Acid-base titration

The acid-base titration was used to determine the pK_a value of the pH-sensitive section in TPPA. In brief, we dissolved 40 mg of PEG-b-P (DEA/D5A) in 3 mL HCl solution (0.1 M) and adjusted the solution volume to 20 mL. Then the solution was titrated by NaOH (0.1 M) under vigorous stirring. The pH changes were monitored using a pH meter (Mettler Toledo S220, Thermo fisher) with a microelectrode. The pK_a was defined as the pH value in the middle of the two equivalent points in the titration curve.

2.4. Transmission electron microscopy (TEM)

1 μg of siRNA was dissolved in 300 μL of nanoparticle stock solution, incubated at room temperature for 15 min, and diluted with 700 μL of HEPES buffer to obtain TPPA/siRNA complex. Briefly, samples were prepared by dipping 10 μL of TPPA/siRNA complex and an equivalent concentration of TPPA (15 mg/mL) onto a carbon-coated copper grid and air-dried before being observed by transmission electron microscopy (Tecnai G2 20 STWIN, Philips, The Netherlands).

2.5. Particle size and Zeta potential characterization

The hydrodynamic diameter and zeta potential of NPs were measured by dynamic light scattering (DLS, Zetasizer Nano ZS90, Malvern Panalytical). The TPPA/siRNA samples (0.1 mg/mL) at different *w*/w ratios were prepared in water. Then a 1 mL sample was analyzed in a matching microcuvette at 25 °C and an incident wavelength of 677 nm. Three measurements were made for each sample.

2.6. pH-sensitivity

The pH sensitivity of TPPA was evaluated using Nile red dye as a fluorescent probe. Briefly, 20 μg of Nile red was dissolved in TPPA polymer (1 mg/mL in PBS, pH = 7.4) to obtain Nile red-loaded micelles through hydrophobic interaction. The pH of the solution was subsequently adjusted to 6.8, 6.4, 6.0, 5.6, 5.2, and 4.8. After incubation for 2 h, the fluorescence intensity was detected by a spectrophotometer (Cary Eclipse, Varian, USA).

2.7. Gel retardation assay

To evaluate the ability of the TPPA vector to encapsulate siRNA, gel electrophoresis experiments were performed. TPPA/siRNA (0.5 μg siRNA) nanocomplexes were prepared at various w/w ratios before mixing with 6× Glycerol Gel Loading Buffer (Sangon Biotech). Then the samples were electrophoresed in a 1% (*w/v*) agarose gel containing 4S Green Plus Nucleic Acid Stain (Sangon Biotech) and in TAE running buffer at 120 V for 20 min.

2.8. Hemolysis analysis

Hemolysis assays were performed to assess the safety and escape effects of TPPA/siRNA in endosomes/lysosomes. Fresh mouse blood (400 μL) was added to two anticoagulant tubes and centrifuged at 10,000 *g* for 5 min at 4 °C. Then the cell pellet was resuspended with 2 mL of pH = 7.4 and pH = 5.5 PBS buffer, respectively. Red blood cell suspension was exposed to 0.8 mL of TPPA/siRNA (15:1, siRNA 0.2 μg/mL) at pH = 7.4 and pH = 5.5. Passive lysis buffer (PLB) was used as a positive control. Samples were incubated at 37 °C for 2 h, then centrifuged at 10,000 *g* for 10 min. The absorbance was measured at 577 nm using a multimode microplate reader (SpectraMax® 190, Molecular Devices) with a reference wavelength of 655 nm. Hemolysis ratio was calculated by $(OD_{(test)} - OD_{(negative\ control)}) / (OD_{(positive\ control)} - OD_{(negative\ control)})$.

2.9. Cytotoxicity analysis (MTT)

MTT was used to assess the viability of cells treated with nanoparticles. HCEC cells or HUVEC cells in logarithmic growth phase were seeded in 96-well plates at 1×10^4 cells/well for 24 h. Cells were transfected with TPPA/siRNA polyplexes at various *w*/w, and the final siRNA concentration was 50 nM. Lipofectamine 2000/siRNA was prepared as a positive control with a fixed volume/weight ratio of 3 μL/1 μg. After 24 h of transfection, all media were removed, and 95 μL fresh complete DMEM and 5 μL MTT (5 mg/mL) were added to each well and incubated for 4 h at 37 °C. Then the solution was gently removed and 50 μL DMSO was added to each well and incubated for another 10 min at 37 °C. When the formazan crystals were completely dissolved, the absorbance was read with a Multi-Mode Microplate Reader (SpectraMax® 190, Molecular Devices) at 540 nm with a reference wavelength of 650 nm, and the absolute absorbance (OD_{net}) was OD_{540} minus OD_{650}. Cell viability was calculated by $OD_{net\ (sample)}/OD_{net\ (control)}$.

2.10. Flow cytometry analysis

Cells were transfected with TPPA/Cy5-siRNA (final siRNA concentration 50 nM) for 4 h. Then Cells were trypsinized with 0.25%, washed three times with cold 1 × PBS (1 mL), suspended in 1 × PBS (400 μL) and detected by flow cytometry (Becton Dickinson, San Jose, CA). The *w*/w ratio of TPPA polymer and siRNA was 15:1 in the following assays.

2.11. Subcellular localization and endosomal escape

HCEC cells were seeded into 35 mm dishes at a density of 2×10^5 cells per well and incubated for 24 h. Then the cells were transfected with TPPA/Cy5-siRNA (15:1, 50 nM) was. After 4 h, cells were washed 3 times with 1 × PBS and treated with100 μL DMEM containing 1 μL Hoechst 33342 (1 mg/mL in PBS, for staining nuclei) and 0.3 μL LysoTracker Green (1:3000 in PBS, for staining endosomes and lysosome). After 30 min of staining, cells were washed twice with 1 × PBS and then recorded with a Zeiss confocal microscope (LSM880, Carl Zeiss, Germany). To analyze the endosomal escape time of PPA/siRNA, cells were stained and imaged according to the above protocol at 4, 6, 10, and 24 h post-transfection, respectively. Images were analyzed using ZEN (ZEN2.3 SP1, Carl Zeiss, Germany).

2.12. Exploring the mechanism of endocytosis

In order to elucidate the endocytic mechanism of TPPA, 100 μM amiloride-HCl (Amil), 30 μM chlorpromazine-HCl (Chlo), 400 μM genistein (Geni), and 5 mM β-cyclodextrin (mβCD) were used to treat HCEC cells for 0.5 h to block macropinocytosis, clathrin-mediated endocytosis, caveolin-mediated endocytosis, and disruption of lipid raft. Cells without inhibitors were used as control. Cells were then co-incubated with TPPA/siRNA NPs, and 4 h post-transfection, cells were analyzed by flow cytometry and microscopy imaging.

2.13. Biodistribution experiment in vivo

Male 6-week-old C57BL/6 mice and BALB/C mice (JieSiJie, Shanghai, China) were used in all experiments. All animal experiments were approved by the Animal Care and Ethics Committee at Wenzhou Medical University. The approval number is "wydw2022–0069".

The distribution and residence time of TPPA/Cy5-siRNA in the eyes of C57BL/6 mice under different administration methods were detected using an *in vivo* imaging system (IVIS, Kodak *In-Vivo* Imaging System FXPro, Carestream Health, USA) and frozen sections. For topical eye drops, firstly, mice were randomly divided into three groups, and 1 μL of PBS, Naked Cy5-siRNA and TPPA/Cy5-siRNA were instilled into the eyes, respectively, and the siRNA concentration was 0.5 mg/mL. Mice dosed subconjunctivally were injected with 10 μL (2.66 μg, C57BL/6) or 20 μL (5.32 μg, BALB/C) of TPPA/Cy5-siRNA (20 μM) per eye.

2.14. Animal models and drug injection

Corneal alkali burns after anesthesia: A 2-mm paper disc containing 1 μL NaOH (1 M) was attached to the center of the cornea for 30 s. Then, we immediately flush the ocular surface along the conjunctiva with 30 ml of normal saline. On day 0, 3, and 6, mice were administered 10 μL of PBS (0.01 M), ranibizumab (21 mg/mL), TPPA/siVEGFA (20 μM, 2.66 μg/dose), or TPPA/siNC (20 μM, 2.66 μg/dose) by subconjunctival injection.

2.15. Cornea clinical evaluation

The images were evaluated for corneal opacity, neovascularization, and vessel size(Yoeruek et al., 2008). Corneal opacity was graded using a scale of 0–4 (0 = completely clear; 1 = slightly hazy, iris and pupils easily visible; 2 = slightly opaque, iris and pupils still detectable; 3 = opaque, pupils hardly detectable; and 4 = completely opaque with no view of the pupils). Neovascularization was graded on a scale of 0–3 (0 = no vessels; 1 = vessels within 1 mm of the corneal limbus; 2 = vessels spanning the corneal limbus; and 3 = vessels spanning the corneal center). Vessel size was scored on a scale of 0–3 (0 = no vessels; 1 = vessels detectable under the microscope; 2 = vessels easily seen under the microscope, and 3 = vessels easily seen without the microscope). Corneal epithelial wound healing was assessed by topical staining with 0.1% sodium fluorescein.

2.16. Corneal flat mounts and immunofluorescence

The cornea was separated and cut into a four-leaf clover shape for tiling. After fixing and blocking, corneas were incubated overnight at 4 °C with an anti-CD31 antibody (rat; 1:500; 553,370; BD Pharmingen, USA), then incubated with Alexa Fluor secondary antibody (A-21209; Thermo Fisher, USA) for 2 h at room temperature. Finally, the corneas were flattened and photographed with a microscope (DM4B, Leica, Germany). Neovascularization area was quantified with ImageJ.

2.17. Morphology analysis

Paraffin slides (5 μm) were stained with hematoxylin and eosin

(H&E) using an autostainer (ST5010, Leica, Germany). Images were acquired using a Leica DM4B microscope.

2.18. Biocompatibility assessment in mice

Fresh submandibular blood samples were collected at the end of the experiment. The blood was centrifuged at 3000 rpm for 10 min, and the supernatant was sent to the partner company (Servicebio, Wuhan, China) for serum biochemical analysis.

2.19. RT-qPCR

The primers were designed using PrimerBank and NCBI, sequences are as follows:

β-ACTIN forward: 5′-CATTGCTGACAGGATGCAGAAGG-3′
β-ACTIN reverse: 5′-TGCTGGAAGGTGGACAGTGAGG-3′
GAPDH forward: 5′-GACTCATGACCACAGTCCATGC-3′
GAPDH reverse: 5′-AGAGGCAGGGATGATGTTCTG-3′
hVEGFA forward: 5′-GCAGCTTGAGTTAAACGAACG-3′
hVEGFA reverse: 5′-GGTTCCCGAAACCCTGAG-3′
mVEGFA forward: 5′-CTGGATATGTTTGACTGCTGTGGA-3′
mVEGFA reverse: 5′-GTTTCTGGAAGTGAGCCAATGTG-3′
mIL-1β forward: 5′-AGAAGGCTGGGGCTCATTTG-3′
mIL-1β reverse: 5′-AGGGGCCATCCACAGTCTTC-3′

2.20. Western blot

Bands were blocked with 5% nonfat milk for 2 h at room temperature. Then, they were incubated with anti-VEGFA antibody (1:1000, ab46154, Abcam, USA) overnight followed by HRP-conjugated secondary antibody for 2 h at room temperature. And α-tubulin was used as an internal control (1:1000; ab24246). Blots were recorded using a multifunctional imaging system (Amersham Imager 680, Cytiva, USA) and analyzed with imageJ.

2.21. Statistics and reproducibility

All data are presented as mean ± SEM, statistics and graphs were performed using GraphPad Prism 8. Statistical significance was tested using one-way ANOVA. In the results, $P < 0.05$ indicated that the difference was statistically significant. ($^{*}P < 0.05$; $^{**}P < 0.01$; $^{***}P < 0.001$).

3. Results

3.1. Synthesis and characterization of TPPA polymer

The triblock polycation $mPEG_{2k}$-$PAMA_{30}$-$P(DEA_{29}$-$D5A_{29})$ (abbreviated as TPPA) was fabricated *via* RAFT polymerization (Fig. S1) and comprised PEG, PAMA, and P(DEA/D5A). PEG was used for anti-protein absorption to extend the cycle time. PAMA was used as a polycationic section to bind siRNA. P(DEA/D5A) exhibits pH-sensitive behavior and enhanced siRNA escape ability(Huang et al., 2019). ^{1}H NMR spectra in Fig. S4 showed that the peaks at 1.8 ppm (f) correspond to the -NCH_2 of the PAMA and P(D5A/DEA). The characteristic peak at 1.6 ppm (g) represents the -CH_2 protons of the P(D5A/DEA) linker. Overall, these NMR findings confirmed the structure of TPPA. Gel permeation chromatography (GPC) results showed that TPPA with a narrow molecular weight distribution (Mw/Mn) of 1.695 (Table. S1).

To investigate the pH-sensitive behavior of the pH-sensitive section in TPPA, acid–base titration was performed (Fig. 1A). We dissolved the PEG-b-P(DEA/D5A) in HCl solution (0.1 M) and adjusted the solution volume to 20 mL, and drop-added NaOH solution. The pK_a value of PEG-b-P(DEA/D5A) was approximately 6.0, which favored charge reversal and siRNA escape in the early endosome pH environment. Moreover, the morphology of TPPA in the dry state was a round sphere, which

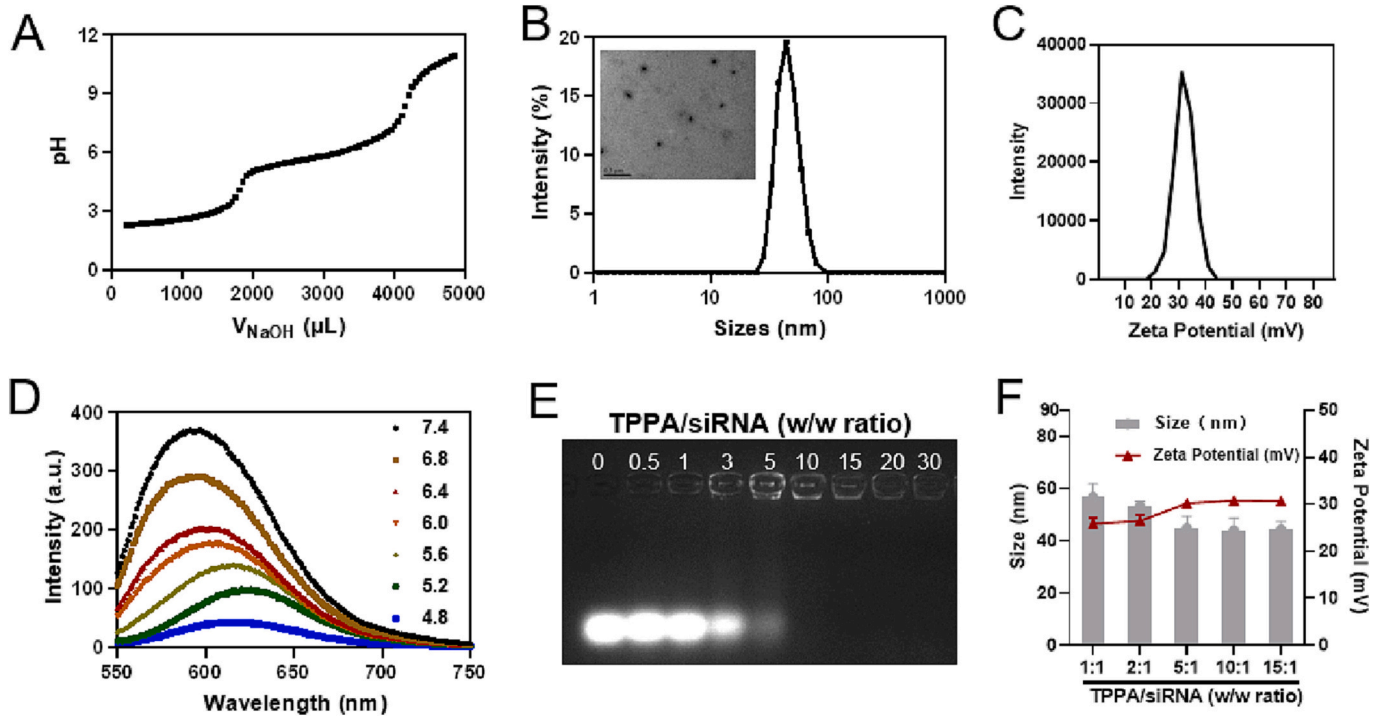

Fig. 1. Characterization of TPPA/siRNA complexes. (A) The pK_a determination of the pH-sensitive section by acid-base titration. (B) The particle size of TPPA. The curve is the hydrodynamic size detected by DLS, and the upper left corner is the morphology map taken by TEM under dry condition. (C) Surface potential (zeta potential) of TPPA detected by DLS. (D) The pH-sensitive assembly/disassembly behavior of TPPA NPs. Nile red dye was used as a fluorescent probe. (E) Agarose gel retardation and (F) Size and zeta potential of TPPA/siRNA complexes at different *w*/w ratios. (For interpretation of the references to colour in this figure legend, the reader is referred to the web version of this article.)

demonstrated that TPPA could assemble into NPs (Fig. 1B). The DLS results showed that the size of the TTPA NPs was approximately 44 nm (Fig. 1B) with a positive charge of 32 mV (Fig. 1C). To verify the pH-sensitive behavior of TPPA NPs, we introduced hydrophobic Nile red as a fluorescence probe. Nile red is a hydrophobic dye whose fluorescence signal weakens when leaving the hydrophobic environment. As shown in Fig. 1D, with the decrease in pH, the fluorescence signal weakens, which is due to the pH-triggered disassembly, resulting in the release of Nile red. The fluorescence signal of Nile red gradually weakens, indicating that TPPA exhibited pH-sensitive disassembly. The siRNA-binding capacity investigated by gel degradation assays showed that TPPA could fully encapsulate and protect siRNA at an *w*/w ratio of 10:1 or higher (Fig. 1E). In a neutral solution, the hydrated particle size of the fully encapsulated complex was stable with a positive surface charge (~30 mV, Fig. 1F). Overall, the results showed that TPPA NPs exhibited not only pH-sensitive behavior but also siRNA-binding ability.

3.2. Enhanced gene silencing of TPPA/siRNA polyplexes

High biocompatibility is an important property of polyplexes. Therefore, the cytotoxicity of TPPA/siRNA polyplexes was investigated. The MTT assay showed that the viability of human corneal epithelial cells (HCECs) and human umbilical vein endothelial cells (HUVECs) treated with TTPA/siRNA were maintained over 80% and 90%, respectively (Fig. 2A and 2D), with no difference compared to those treated with Lipo 2000. Considering that the *w*/w ratio affects not only the encapsulation ability but also the stability and biodistribution of polyplexes (Phillips et al., 2019), the relationship between gene silencing and the w/w ratio was explored. RT–qPCR was used to assess the gene silencing efficiency of TPPA with siRNA targeting VEGFA, which has been proven to be the primary regulator of CoNV (Giannaccare et al., 2020; Roshandel et al., 2018; Sene et al., 2015). Results showed that higher w/w ratios induced lower VEGFA mRNA expression in HCECs (Fig. 2C). Notably, at w/w = 15/1, the inhibition ratio of TPPA/siVEGFA was comparable to Lipo 2000 (57.07% *vs* 52.8%). TPPA could deliver siRNA into HUVECs cytoplasm at a low w/w ratio, and the silencing effect was similar to Lipo 2000 when w/w was 15/1 (72.73% *vs* 74.66%, Fig. 2D). Subsequently, we investigated VEGFA protein inhibition by TPPA/siVEGFA (*w*/w: 15/1) with different siVEGFA concentrations. As shown in Figs. 2E and F, the protein levels of VEGFA showed siVEGFA concentration dependence, and w/w 15:1 and 50 nM siRNA were used in the following study. Overall, TPPA vehicles possessed the ability to deliver siRNA into the cytoplasm to silence VEGFA expression.

3.3. Internalization and cellular trafficking of TPPA/siRNA polyplexes

Cellular uptake and early endosome escape are the main factors affecting effective gene effectively delivery (Nóbrega et al., 2020). Motivated by efficient VEGFA silencing, cell uptake was determined by flow cytometry and microscope. Flow cytometry data demonstrated that cells were 100% Cy5 positive after TPPA/Cy5-siRNA treatment, which was greater than Lipo 2000/Cy5-siRNA (91.2%), suggesting that TPPA/siRNA was internalized in all cells (Fig. 3A). Furthermore, the mean fluorescence intensity (MFI) demonstrated that the cellular uptake efficiency of TPPA/siVEGFA nanomicelles was 4.25 times greater than that of Lipo 2000/siVEGFA (1.67 × 104 *vs* 7.10 × 104, Fig. 3C). The microscope results further confirmed the higher endocytosis efficiency of the TPPA/Cy5-siRNA (Figs. 3F, G). The small sizes and positive surface charge of TPPA/siRNA polyplexes were important in enhancing endocytosis efficiency (Augustine et al., 2020).

The endocytic pathway was evaluated to further investigate the reason for the high cellular uptake of the TPPA/siRNA polyplexes. Cells with a positive fluorescence signal decreased from 100% to 77.9% in the

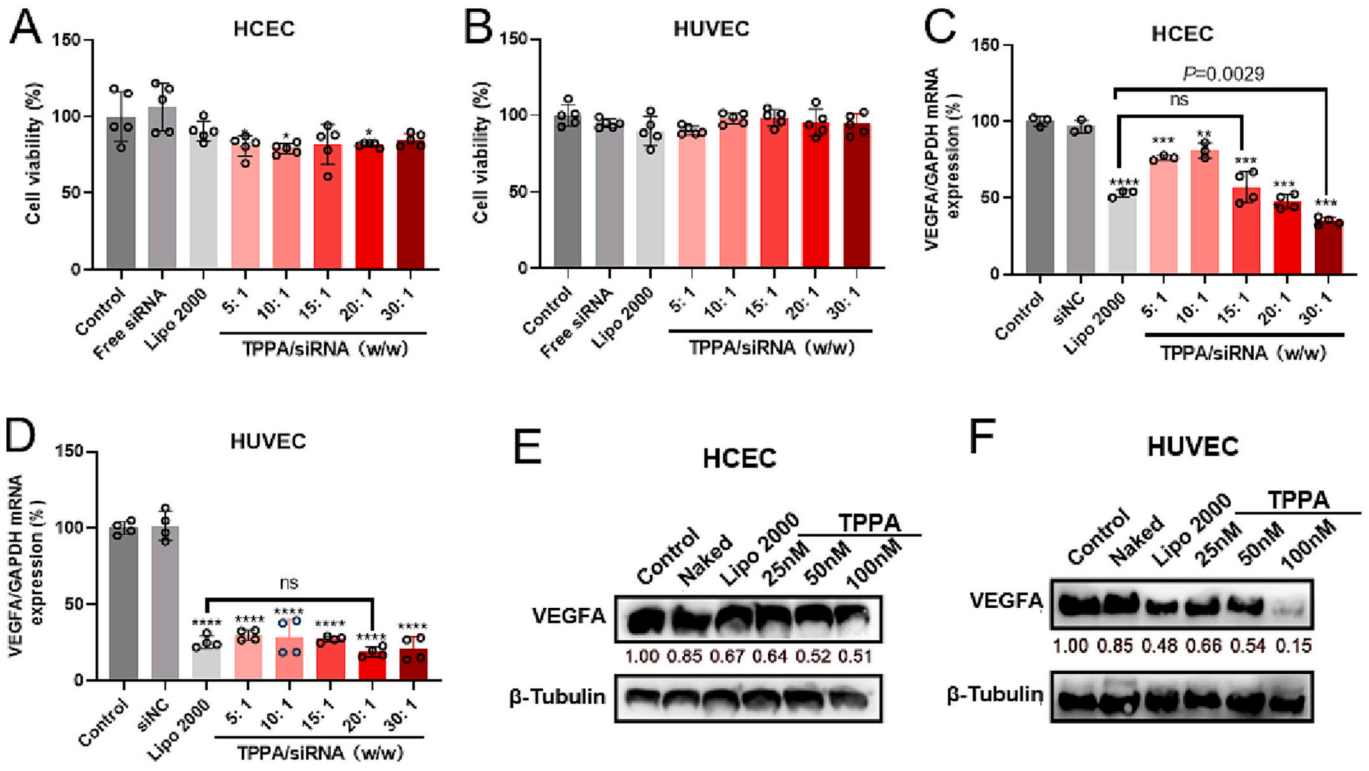

Fig. 2. *In vitro* performance of TPPA/siRNA polyplexes. (A) Cell viability of HCEC cells and (B) HUVEC cells evaluated by MTT assay 24 h after the transfection of TPPA/siRNA. Lipofectamine 2000 abbreviated Lipo 2000 was used as a positive control. (C) Relative VEGFA mRNA expression of HCEC cells and (D) HUVEC cells after TPPA/siRNA treatment. (E) VEGFA protein expression of HCEC cells and (F) HUVEC cells evaluated by western blot. The numbers in the figure represent the grayscale value. $^{*}P < 0.05$, $^{**}P < 0.01$, $^{***}P < 0.001$.

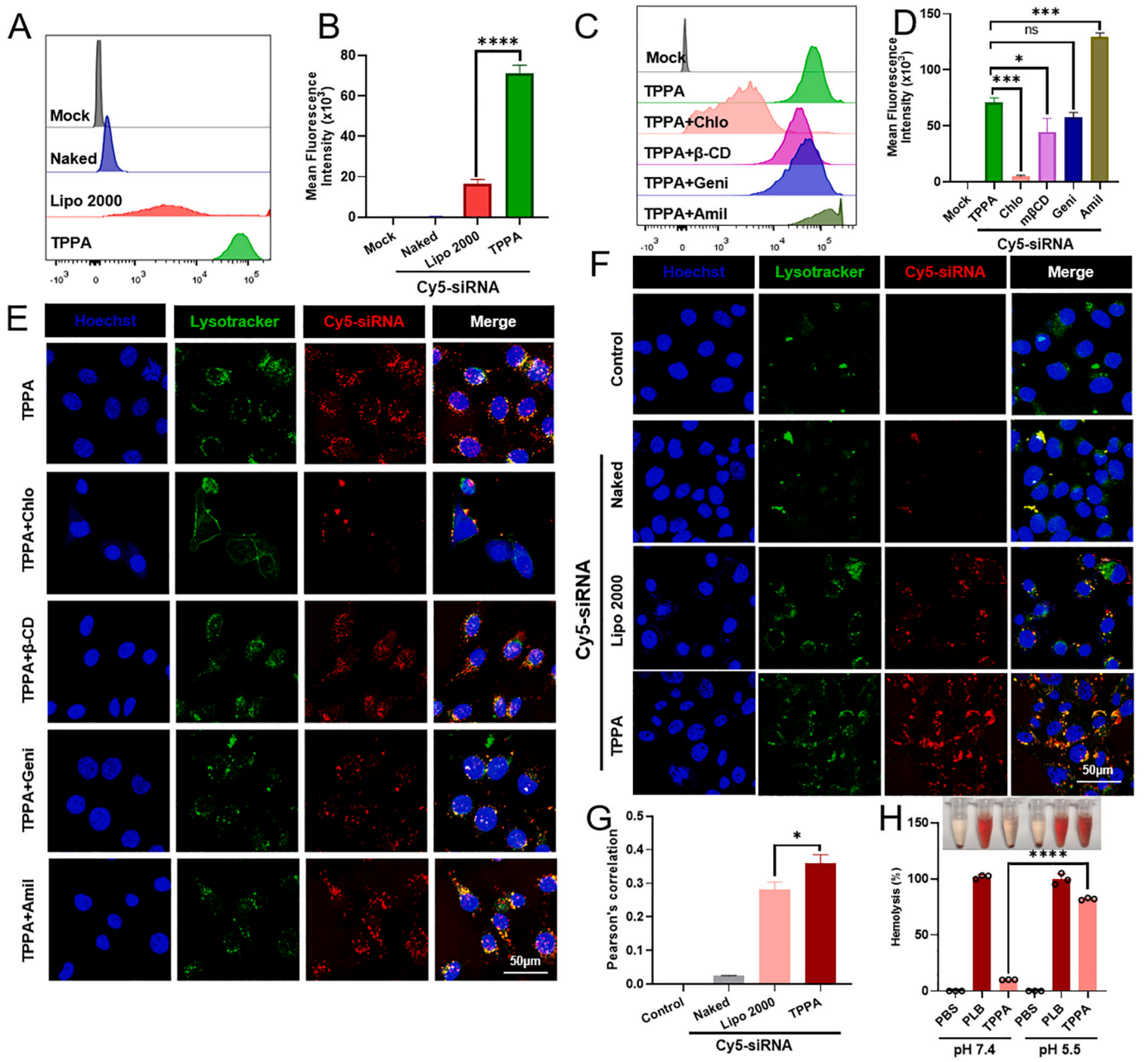

Fig. 3. Endosomal escaping and cell internalization of TPPA/siRNA. (A) Flow cytometry histogram of HCEC cells after treatment with TPPA/Cy5-siRNA complexes. (B) Cellular uptake of TPPA/Cy5-siRNA represented by mean fluorescence intensity (MFI) of panel A. (C) Flow cytometry histogram of HCEC cells after treatment with TPPA/Cy5-siRNA and different endocytosis inhibitors. Amiloride inhibits macropinocytosis; chlorpromazine inhibits clathrin-mediated endocytosis; genistein inhibits caveolin-mediated endocytosis, and β-cyclodextrin disrupts lipid raft. (D) MFI analysis of panel D. (E) Confocal images of TPPA/Cy5- siRNA complexes in the HCEC cells with different inhibitors. Scale bar, 50 μm. (F) Fluorescence microscopy images of HCEC cells 24 h after transfecting Cy5-siRNA (*red*). LysoTracker (*green*) was used to label endosomes and lysosomes. Hoechst 33342 (*blue*) represents the cell nuclear. Scale bar, 50 μm. (G) Colocalization analysis of Cy5-siRNA (*red*) and LysoTracker (*green*) in panel F. (H) Hemolysis ratio of TPPA in different pH. Passive lysis buffer (PLB) was used as positive control. (For interpretation of the references to colour in this figure legend, the reader is referred to the web version of this article.)

Chlo-treated group, while other inhibitors showed a slight influence on cellular uptake (Fig. 3C). At the same time, other inhibitors showed a slight influence on cellular uptake (Fig. 3C). According to the MFI analysis, the fluorescence intensity after Chlo treatment was 13.24 times lower than that without inhibitor (4.98 × 105 *vs* 70.9 × 105, Fig. 3D). The Cy5 fluorescence intensity of the Geni and mβCD groups showed a decreasing trend. The Cy5-siRNA signal in the Amil group was 0.8 times higher than TPPA/Cy5-siRNA, which is discussed below. In addition, the internalization was shown by microscope (Fig. S5A, B). The Cy5 fluorescence signal remained stable until 24 h, with a signal 2.48 times higher than that at 1 h. In summary, the results proved that clathrin-mediated endocytosis dominated in the high endocytosis efficiency of TPPA/siRNA polyplex.

Subsequently, the escape ability of TPPA/Cy5-siRNA was examined. Less red signal was present in the cytoplasm in the TPPA/Cy5-siRNA group than Lipo 2000(Fig. 3F), the colocalization ratio of TPPA/Cy5-siRNA polyplexes was higher than that of Lipo 2000/siRNA (0.36 *vs* 0.28, Fig. 3G). Additionally, there was no significant change in the colocalization ratio over time (Fig. S5C). Next, we tested the biosafety of TPPA/siRNA and found that TPPA caused little hemolysis at pH 7.4 but

efficiently mediated hemolysis (82%) at pH 5.5 (Fig. 3 h). TPPA is safe in normal physiological environments but can easily destroy membranes in acidic mature endosomes. Overall, the higher endocytosis efficiency and lower escape ability of TPPA/siRNA resulted in considerable gene silencing efficiency, similar to Lipo 2000.

3.4. Corneal distribution of TPPA /siRNA polyplexes

To determine the biodistribution *in vivo*, two common local administrations, eye drops and subconjunctival injection (Kutlehria et al., 2018; Li et al., 2015; Wilson, 2022), were administered . IVIS imaging showed that the naked Cy5-siRNA signal decreased rapidly, and no signal was observed at 0.5 h after topical treatment in the extracted eyeballs (Fig. 4A). Notably, the fluorescence signal of TPPA/Cy5-siRNA decreased slowly and could be detected for up to 4 h. Cryostat sections at 0.5 and 4 h were made and maintained in line with the *in vivo* imaging data (Fig. 4 and Fig. S7). The TPPA/siRNA signal was observed in corneal epithelium cells for as long as 4 h, while no signal was detected in the naked siRNA group, indicating that TPPA could effectively prolong retention time and facilitate penetration into the corneal epithelium.

Subconjunctival injection is more beneficial than eye drops for drug delivery to the cornea's inner layers (such as the stroma and endothelium) and can achieve a longer therapeutic effect. Considering that neovascularization was mainly distributed in the stromal layer, we analyzed the corneal distribution of TPPA/siRNA administered *via* subconjunctival injection. As shown in Fig. 4C, the signal of TPPA/Cy5-siRNA was detected for up to 72 h, while the naked Cy5-siRNA signal disappeared within 24 h. The difference was more intuitive in BABL mice without melanin (Fig. S7). Cryostat sections revealed that the Cy5-siRNA signal was evenly distributed to the full layers of the cornea (for <4 h) and maintained a wide distribution for as long as 72 h. The MFI of Cy5-siRNA did not decrease until 72 h (Fig. 4E), so subconjunctival injection was used for therapeutic experiments. These data showed that TPPA exhibited extensive and sustained dispersion due to mucoadhesion, small size, and high cellular uptake.

3.5. TPPA /siVEGFA polyplexes inhibit mice CoNV

To explore the *in vivo* anti-angiogenic effects of TPPA, we constructed a mouse model of alkali-burn-induced CoNV, a common clinical ocular emergency that results in severe corneal damage and neovascularization. Three conjunctival injection doses were administered on days 0, 3, and 6 post-modeling. As shown in Fig. 5, progressive neovascularization developed in the corneas of mice treated with PBS (passive control) and clinical scores was stable. From day 3, the anti-VEGF drug ranibizumab group showed an inhibitory effect on the area of corneal injury (Fig. 5F, L). However, there was no difference in the vascular score, which may be mainly related to the vary accuracy of different methods. On day 7, the clinical score decreased significantly (Fig. 5K). Importantly, TPPA/siRNA achieved a therapeutic effect that was not significantly different from ranibizumab. The data indicated that TPPA could effectively deliver a sufficient amount of siVEGFA into the target cells and play a role in anti- CoNV *in vivo*.

Next, we evaluated the anti-vascular effects and molecular mechanisms of TPPA/siRNA at the tissue and molecular biological levels. Fewer vessels (marked by CD31) were observed in the fluorescence images with ranibizumab or TPPA/siVEGFA administration (Fig. 6A). Quantitative results showed that compared with PBS, the areas of neovascularization in the ranibizumab and TTPA/siVEGFA groups were reduced by 42.27% ($P = 0.0023$) and 33.66% ($P = 0.0161$), respectively (Fig. 6B). This decrease was not significantly different between the TPPA/siRNA and ranibizumab groups. Furthermore, histomorphological examination (H&E staining) showed no obvious blood vessels were found after TPPA/siVEGFA or ranibizumab treatment (Fig. 6A). There was also no significant difference between TPPA/siRNA and ranibizumab, revealing similar anti-angiogenic effects. Our data confirmed the inhibition of neovascularization by TPPA/siRNA at the tissue level.

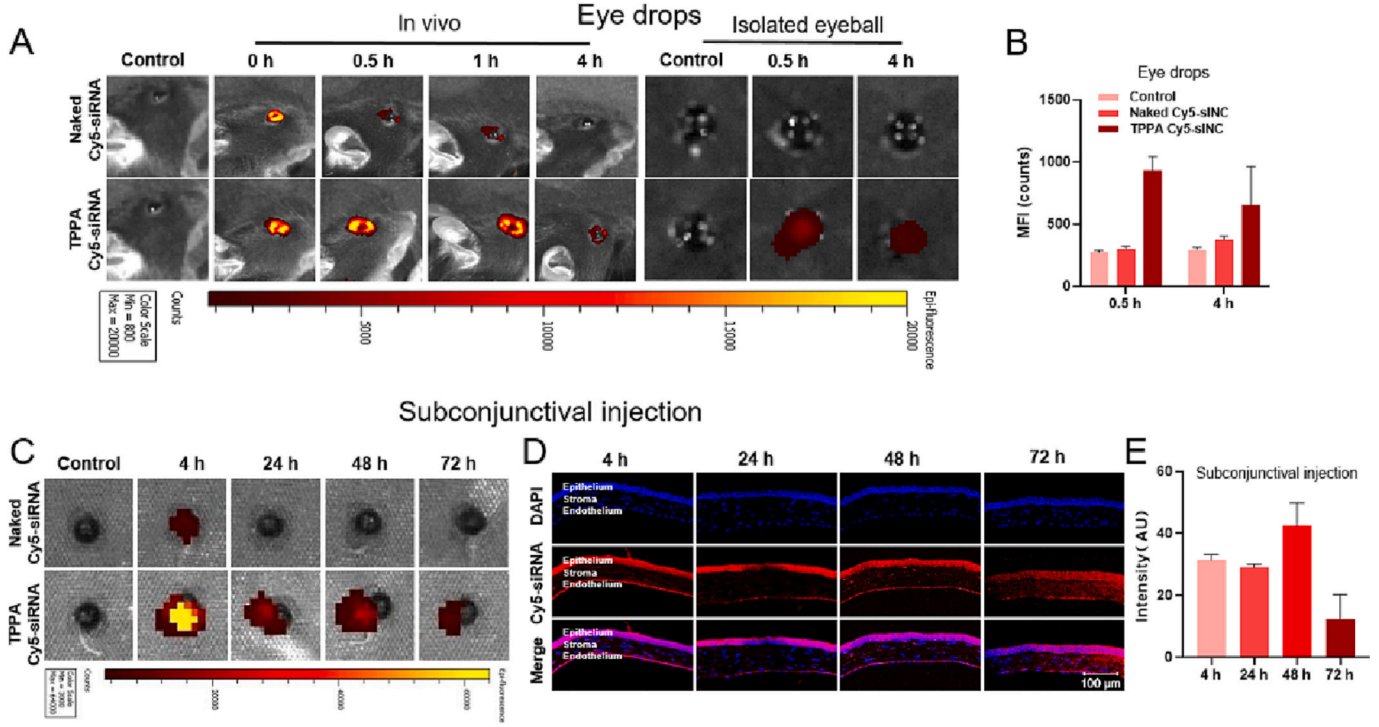

Fig. 4. Biodistribution of TPPA/siRNA polyplexes with topical treatment (A-B) and subconjunctival injection (C-E). (A) IVIS imaging after topical treatment of TPPA/Cy5-siRNA. (B) Quantification of eyeballs in panel A. (C) IVIS images after subconjunctival injection. (D) Corneal sections 4 h, 24 h, and 72 h after subconjunctival injection. (E) Quantification of panel D. AU: Arbitrary Units.

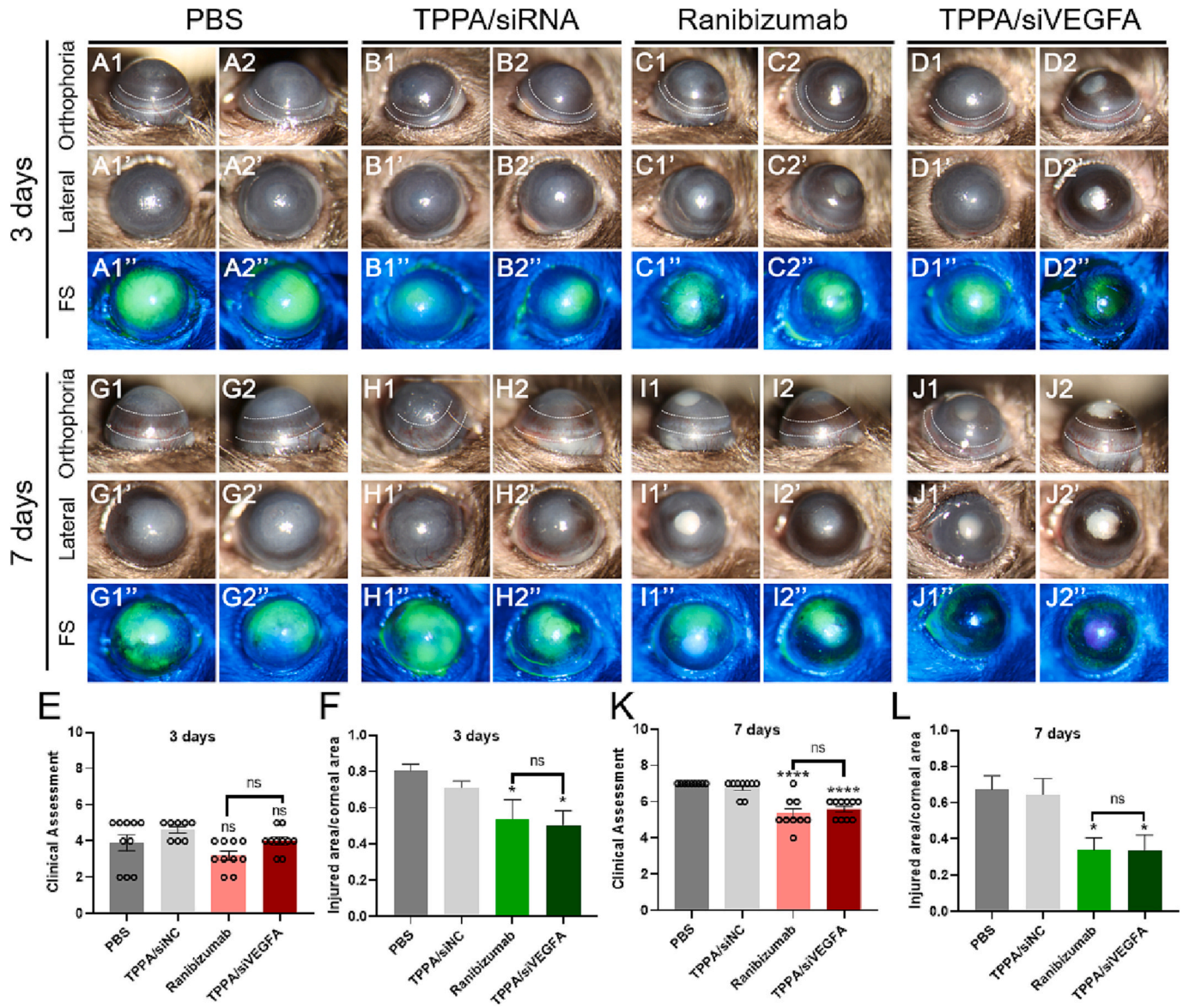

Fig. 5. Anti-neovascular effect of TPPA/siVEGFA in alkali corneal burn model. (A1-D2") Slit-lamp images three days after alkali burn. A1 and A2 are different samples treated with PBS, and A1, A1', and A1" are different images of the same sample. The *white dotted line* represents the extent of the vascular. FS: fluorescein sodium staining, marking the corneal injury area. Ranibizumab was used as the positive control drug. (E) Clinical score and (F) injury area statistics three days after alkali burn. (G1-L) Slit-lamp images and analyses seven days after alkali burn.

To confirm that the *in vivo* anti-vascular effect of the polyplexes was induced by siVEGFA rather than an off-target effect, we examined the mRNA and protein expression of VEGFA in the cornea. RT-qPCR analysis revealed that VEGFA expression was downregulated after TPPA/siVEGFA treatment (Fig. 6C). Notably, ranibizumab did not show the same inhibition at the transcriptional level, probably owing to the inherent properties of the antibodies themselves. Western blot analysis showed that VEGFA protein levels decreased in both the ranibizumab and TPPA/siVEGFA treatment groups, with no significant difference between the two groups (Fig. 6D, E). These results verified that TPPA/siVEGFA effectively reduces VEGFA and thus, anti-angiogenesis in mice.

3.6. Biocompatibility

Inflammatory factors and inflammatory cell infiltration in the cornea were examined to assess the local toxicity of the polyplexes. H&E images showed that inflammatory cell infiltration decreased and corneal edema alleviated with ranibizumab or TPPA/siVEGFA treatment (Fig. 6A). However, a slight downregulation ($P = 0.16$) of TNFα expression was observed only with ranibizumab treatment (Fig. S8). This suggests that TPPA/siVEGFA is slightly less effective than ranibizumab in reducing inflammation, but no significant difference was found. To be prudent, possible systemic toxicity was further explored using hematological analysis of liver, kidney, and heart function and histological analysis of major organs (the heart, liver, spleen, lung, and kidney). As shown in Fig. S6, the TPPA/siRNA complex had no effect on the function and morphology of other organs in the body and no systemic toxicity.

4. Discussion

In this study, we aimed to develop a new strategy using siVEGFA to silence VEGFA for CoNV treatment. Our findings in the mouse CoNV model showed a favorable therapeutic effect of TPPA/siVEGFA treatment, a finding supported by the high cellular uptake rate, high silencing efficiency, extensive diffusion, and long-term retention (Figs. 2–4). Similar to elastic nanoparticles, the process of polymers entering cells is

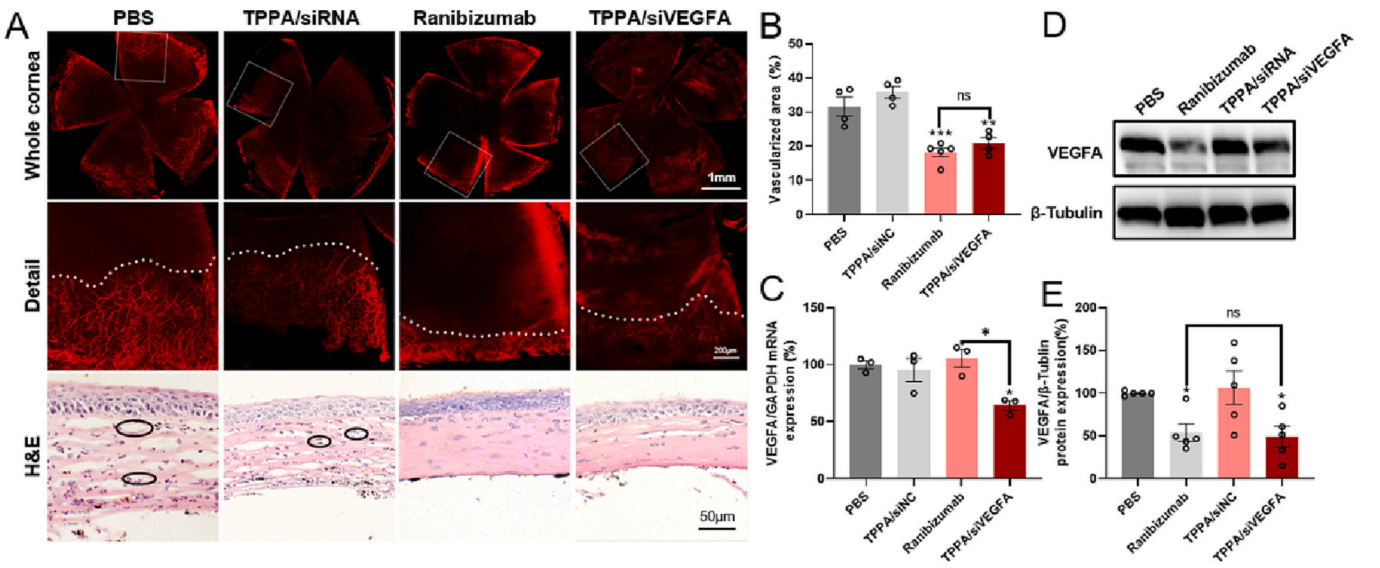

Fig. 6. Anti-neovascular and biocompatibility assessment of TPPA/siVEGFA in mouse model. (A) Whole mount immunofluorescence pictures and HE sections of cornea. The first row is a picture of vascular staining of the whole cornea marked with CD31 (*red*); the second row is a magnified image of the outlined region in the first row; and the third row is a H&E staining of a paraffin section with blood vessels circled by *black ovals*. (B) Quantitative statistical results of panel A. (C) VEGFA mRNA expression detected by RT-qPCR. (D)WB and (E)grayscale analysis determined the protein level of cornea VEGFA. (For interpretation of the references to colour in this figure legend, the reader is referred to the web version of this article.)

affected by many factors, including receptor–ligand interaction, chemical composition, surface charge, surface adsorption energy, shape, size, elastic properties, and other multi-dimensional characteristics (Augustine et al., 2020; Shen et al., 2019; Zhang et al., 2015). Surface charge and size are the most commonly considered factors that affect nanoparticle internalization. Nanoparticles with a high positive surface charge and small size are conducive to cellular uptake (Augustine et al., 2020; Weng et al., 2018). On the corneal surface, the high surface potential (+32 mV) and physical mucoadhesion of the TPPA/siRNA micelles enhance interactions with negatively charged mucins and corneal cells, thereby extending retention time. Corneal penetration and retention time are the greatest challenges in ocular surface administration. Small particles (<50 nm) facilitate corneal penetration and distribution. Small nanoparticles are more evenly distributed on the surface of the eye (Weng et al., 2018) and can pass through the corneal barrier more easily. In addition, their small size facilitates cellular uptake, and cell-to-cell communication can transport the polymers to further tissues, which is also important for subconjunctival drug delivery.

We speculate that the pH sensitivity of TPPA plays an important role in its cellular uptake and tissue targeting. Many studies have found that pH-sensitivity promotes the cellular uptake of nanoparticles. For example, pH-sensitive polyethylenimine (PEI) exhibited higher transfection efficiency than non-pH-sensitive PEI (Chandrashekhar et al., 2013). Moreover, Zhao (Zhao et al., 2022) reported that pH-responsive peptide facilitated cellular uptake. CoNV has a slightly acidic pathological microenvironment. The pH of the cornea stabilized at ~6.9 after alkali burn, which is lower than the pre-burn pH (~7.3) (Paschalis et al., 2017; Roshandel et al., 2018). This means that pH-responsive TPPA exhibits a stronger positive charge at the site of keratopathy, which facilitates targeted aggregation of the polymer in the lesion. Based on *in vitro* and *in vivo* experiments, we speculate that pH-responsiveness, positive charge, small size, and physical viscosity are the causes of corneal siRNA delivery optimization of TPPA.

One or more of these mechanisms generally dominate the cellular uptake of polymer vehicles (Weng et al., 2019). In this study, amiloride treatment facilitated the internalization of TPPA/siRNA. Amiloride is a macropinocytosis inhibitor that works by reducing intracellular pH and extracellular alkalization (Cheng et al., 2019; Koivusalo et al., 2010; Lin and Huang, 2022), meaning that the cell has stronger electrostatic adsorption to positively charged polymer particles through other endocytosis pathways, such as clathrin-mediated endocytosis, as shown in our data. In addition, Geng et al. (Geng et al., 2012) found that amiloride could promote the entry of DNA into cells, although the mechanism is unknown. Clinically, amiloride is a conventional drug used to combat hypertension; therefore, the promoting effect of amiloride on internalization requires further study to clarify its characteristics and mechanism.

5. Conclusion

In our study, the performance and mechanism of TPPA polymers for siRNA delivery were comprehensively and systematically evaluated. The pH-responsive structure and high cellular uptake rate highlighted TPPA as an excellent carrier superior to commercial Lipo 2000 *in vitro*. The primary mechanism of TPPA/siRNA is clathrin-mediated endocytosis. In a CoNV mouse model, TPPA/siVEGFA achieved a similar anti-angiogenic effect to ranibizumab. From biosafety perspective, a combination of anti-inflammatory drugs may facilitate its clinical application. In general, TPPA is an ideal gene carrier, with a simple synthesis process and high gene silencing efficiency, with the potential to be developed into clinical drugs to treat CoNV. In addition, this study provides a reference for the rational design of block copolymers for siRNA delivery and anti-angiogenesis studies.

Author contributions

HC supervised the project; HC and XC designed research and methodology. CW synthesized the material. XC, DZ and YZ performed and analyzed the cell and animal experiments. HC, CW and XC wrote and revised the manuscript. All authors reviewed the manuscript for submission.

Declaration of Competing Interest

The authors report no conflict of interest.

Data availability

No data was used for the research described in the article.

Acknowledgments

This study was supported by Wenzhou High-level Innovation Team Project and the Initiation Project of internal science research in the affiliated Ophthalmology Hospital of Wenzhou Medical University (No. KJYN0571, China). The author would like to thank the help from Dr. Yuhua Weng (Beijing Institute of Technology, Beijing, China).

Appendix A. Supplementary data

Supplementary data to this article can be found online at https://doi.org/10.1016/j.ijpx.2023.100183.

References

Arbabi, A., Liu, A., Ameri, H., 2019. Gene Therapy for Inherited Retinal Degeneration. J. Ocul. Pharmacol. Ther. 35, 79–97.
Asayama, S., Sudo, M., Nagaoka, S., Kawakami, H., 2008. Carboxymethyl poly(L-histidine) as a new pH-sensitive polypeptide to enhance polyplex gene delivery. Mol. Pharm. 5, 898–901.
Augustine, R., Hasan, A., Primavera, R., Wilson, R.J., Thakor, A.S., Kevadiya, B.D., 2020. Cellular uptake and retention of nanoparticles: insights on particle properties and interaction with cellular components. Mater. Today Commun. 25.
Baran-Rachwalska, P., Torabi-Pour, N., Sutera, F.M., Ahmed, M., Thomas, K., Nesbit, M. A., Welsh, M., Moore, C.B.T., Saffie-Siebert, S.R., 2020. Topical siRNA delivery to the cornea and anterior eye by hybrid silicon-lipid nanoparticles. J. Control. Release 326, 192–202.
Chandrashekhar, C., Pons, B., Muller, C.D., Tounsi, N., Mulherkar, R., Zuber, G., 2013. Oligobenzylethylenimine enriches linear polyethylenimine with a pH-sensitive membrane-disruptive property and leads to enhanced gene delivery activity. Acta Biomater. 9, 4985–4993.
Chen, H., Zhang, H., Thor, D., Rahimian, R., Guo, X., 2012. Novel pH-sensitive cationic lipids with linear ortho ester linkers for gene delivery. Eur. J. Med. Chem. 52, 159–172.
Cheng, P.C., Lin, H.Y., Chen, Y.S., Cheng, R.C., Su, H.C., Huang, R.C., 2019. The Na(+/)H(+)-Exchanger NHE1 regulates extra- and intracellular ph and nimodipine-sensitive [Ca(2+)](i) in the suprachiasmatic nucleus. Sci. Rep. 9, 6430.
Chu, C., Yu, J., Ren, E., Ou, S., Zhang, Y., Wu, Y., Wu, H., Zhang, Y., Zhu, J., Dai, Q., Wang, X., Zhao, Q., Li, W., Liu, Z., Chen, X., Liu, G., 2020. Multimodal photoacoustic imaging-guided regression of corneal neovascularization: a non-invasive and safe strategy. Adv. Sci. (Weinh) 7, 2000346.
Du, L., Wang, C., Meng, L., Cheng, Q., Zhou, J., Wang, X., Zhao, D., Zhang, J., Deng, L., Liang, Z., Dong, A., Cao, H., 2018. The study of relationships between pKa value and siRNA delivery efficiency based on tri-block copolymers. Biomaterials 176, 84–93.
Feizi, S., Azari, A.A., Safapour, S., 2017. Therapeutic approaches for corneal neovascularization. Eye Vis. (Lond.) 4, 28.
Fernando, O., Tagalakis, A.D., Awwad, S., Brocchini, S., Khaw, P.T., Hart, S.L., Yu-Wai-Man, C., 2018. Development of targeted siRNA nanocomplexes to prevent fibrosis in experimental glaucoma filtration surgery. Mol. Ther. 26, 2812–2822.
Geng, S., Zhong, Y., Wang, S., Liu, H., Zou, Q., Xie, X., Li, C., Yu, Q., He, Z., Wang, B., 2012. Amiloride enhances antigen specific CTL by faciliting HBV DNA vaccine entry into cells. PLoS One 7, e33015.
Giannaccare, G., Pellegrini, M., Bovone, C., Spena, R., Senni, C., Scorcia, V., Busin, M., 2020. Anti-VEGF treatment in corneal diseases. Curr. Drug Targets 21, 1159–1180.
Gupta, D., Illingworth, C., 2011. Treatments for corneal neovascularization: a review. Cornea 30, 927–938.
Huang, W., Wang, X., Wang, C., Du, L., Zhang, J., Deng, L., Cao, H., Dong, A., 2019. Structural exploration of hydrophobic core in polycationic micelles for improving siRNA delivery efficiency and cell viability. J. Mater. Chem. B 7, 965–973.
Kim, T.W., Lindsey, J.D., Aihara, M., Anthony, T.L., Weinreb, R.N., 2002. Intraocular distribution of 70-kDa dextran after subconjunctival injection in mice. Invest. Ophthalmol. Vis. Sci. 43, 1809–1816.
Koivusalo, M., Welch, C., Hayashi, H., Scott, C.C., Kim, M., Alexander, T., Touret, N., Hahn, K.M., Grinstein, S., 2010. Amiloride inhibits macropinocytosis by lowering submembranous pH and preventing Rac1 and Cdc42 signaling. J. Cell Biol. 188, 547–563.
Kutlehria, S., Vhora, I., Bagde, A., Chowdhury, N., Behl, G., Patel, K., Singh, M., 2018. Tacrolimus Loaded PEG-Cholecalciferol Based Micelles for Treatment of Ocular Inflammation. Pharm. Res. 35, 117.
Kwak, G., Jo, S.D., Kim, D., Kim, H., Kim, M.G., Kim, K., Kwon, I.C., Kim, 2018. S.H., n.d. Synergistic Antitumor Effects of Combination Treatment with Metronomic Doxorubicin and VEGF-Targeting RNAi Nanoparticles. J Control Release 267, 203–213.
Lee, P., Wang, C.C., Adamis, A.P., 1998. Ocular neovascularization: an epidemiologic review. Surv. Ophthalmol. 43, 245–269.
Li, J., Li, Z., Zhou, T., Zhang, J., Xia, H., Li, H., He, J., He, S., Wang, L., 2015. Positively charged micelles based on a triblock copolymer demonstrate enhanced corneal penetration. Int. J. Nanomedicine 10, 6027–6037.
Li, C., Zhou, J., Wu, Y., Dong, Y., Du, L., Yang, T., Wang, Y., Guo, S., Zhang, M., Hussain, A., Xiao, H., Weng, Y., Huang, Y., Wang, X., Liang, Z., Cao, H., Zhao, Y., Liang, X.J., Dong, A., Huang, Y., 2021. Core Role of Hydrophobic Core of Polymeric Nanomicelle in Endosomal Escape of siRNA. Nano Lett. 21, 3680-3689.
Lin, H.Y., Huang, R.C., 2022. Glycolytic metabolism and activation of Na(+) pumping contribute to extracellular acidification in the central clock of the suprachiasmatic nucleus: Differential glucose sensitivity and utilization between oxidative and non-oxidative glycolytic pathways. Biom. J. 45, 143–154.
Nóbrega, C., Mendonça, L., Matos, C.A., 2020. Non-viral Vectors for Gene Therapy. In: Nóbrega, C., Mendonça, L., Matos, C.A. (Eds.), A Handbook of Gene and Cell Therapy. Springer International Publishing, Cham, pp. 23–37.
Park, W., Shin, H., Choi, B., Rhim, W.-K., Na, K., Keun Han, D., 2020. Advanced hybrid nanomaterials for biomedical applications. Prog. Mater. Sci.114, 10068.
Paschalis, E.I., Zhou, C., Lei, F., Scott, N., Kapoulea, V., Robert, M.C., Vavvas, D., Dana, R., Chodosh, J., Dohlman, C.H., 2017. Mechanisms of RETINAL DAMAGE AFTER OCULAR ALKALI BUrns. Am. J. Pathol. 187, 1327–1342.
Phillips, H.R., Tolstyka, Z.P., Hall, B.C., Hexum, J.K., Hackett, P.B., Reineke, T.M., 2019. Glycopolycation-DNA polyplex formulation N/P ratio affects stability, hemocompatibility, and in vivo biodistribution. Biomacromolecules 20, 1530–1544.
Roshandel, D., Eslani, M., Baradaran-Rafii, A., Cheung, A.Y., Kurji, K., Jabbehdari, S., Maiz, A., Jalali, S., Djalilian, A.R., Holland, E.J., 2018. Current and emerging therapies for corneal neovascularization. Ocul. Surf. 16, 398–414.
Semple, S.C., Akinc, A., Chen, J., Sandhu, A.P., Mui, B.L., Cho, C.K., Sah, D.W., Stebbing, D., Crosley, E.J., Yaworski, E., Hafez, I.M., Dorkin, J.R., Qin, J., Lam, K., Rajeev, K.G., Wong, K.F., Jeffs, L.B., Nechev, L., Eisenhardt, M.L., Jayaraman, M., Kazem, M., Maier, M.A., Srinivasulu, M., Weinstein, M.J., Chen, Q., Alvarez, R., Barros, S.A., De, S., Klimuk, S.K., Borland, T., Kosovrasti, V., Cantley, W.L., Tam, Y. K., Manoharan, M., Ciufolini, M.A., Tracy, M.A., de Fougerolles, A., MacLachlan, I., Cullis, P.R., Madden, T.D., Hope, M.J., 2010. Rational design of cationic lipids for siRNA delivery. Nat. Biotechnol. 28, 172–176.
Sene, A., Chin-Yee, D., Apte, R.S., 2015. Seeing through VEGF: innate and adaptive immunity in pathological angiogenesis in the eye. Trends Mol. Med. 21, 43–51.
Shen, Z., Ye, H., Yi, X., Li, Y., 2019. Membrane Wrapping Efficiency of Elastic Nanoparticles during Endocytosis: size and Shape Matter. ACS Nano 13, 215–228.
Truong, N.P., Gu, W., Prasadam, I., Jia, Z., Crawford, R., Xiao, Y., Monteiro, M.J., 2013. An influenza virus-inspired polymer system for the timed release of siRNA. Nat. Commun. 4, 1902.
Upadhya, R., Kosuri, S., Tamasi, M., Meyer, T.A., Atta, S., Webb, M.A., Gormley, A.J., 2020. Automation and data-driven design of polymer therapeutics. Adv. Drug Deliv. Rev. 171, 1-28.
Wang, C., Du, L., Zhou, J., Meng, L., Cheng, Q., Wang, C., Wang, X., Zhao, D., Huang, Y., Zheng, S., Cao, H., Zhang, J., Deng, L., Liang, Z., Dong, A., 2017. Elaboration on the distribution of hydrophobic segments in the chains of amphiphilic cationic polymers for small interfering RNA delivery. ACS Appl. Mater. Interfaces 9, 32463–32474.
Wang, C., Wang, X., Du, L., Dong, Y., Hu, B., Zhou, J., Shi, Y., Bai, S., Huang, Y., Cao, H., Liang, Z., Dong, A., 2021. Harnessing pH-sensitive polycation vehicles for the efficient siRNA delivery. ACS Appl. Mater. Interfaces 13, 2218–2229.
Wels, M., Roels, D., Raemdonck, K., De Smedt, S.C., Sauvage, F., 2021. Challenges and strategies for the delivery of biologics to the cornea. J. Control. Release 333, 560–578.
Weng, Y., Xiao, H., Zhang, J., Liang, X.J., Huang, Y., 2019. RNAi therapeutic and its innovative biotechnological evolution. Biotechnol. Adv. 37, 801–825.
Weng, Y.H., Ma, X.W., Che, J., Li, C., Liu, J., Chen, S.Z., Wang, Y.Q., Gan, Y.L., Chen, H., Hu, Z.B., Nan, K.H., Liang, X.J., 2018. Nanomicelle-assisted targeted ocular delivery with enhanced antiinflammatory efficacy in vivo. Adv. Sci. (Weinh) 5, 1700455.
Wilson, S.E., 2022. Magic Bullets: The Coming Age of Meaningful Pharmacological Control of the Corneal Responses to Injury and Disease. J. Ocul. Pharmacol. Ther. 38, 594–606.
Wilson, R.C., Doudna, J.A., 2013. Molecular mechanisms of RNA interference. Annu. Rev. Biophys. 42, 217–239.
Xu, R., Lu, Z.-R., 2011. Design, synthesis and evaluation of spermine-based pH-sensitive amphiphilic gene delivery systems: Multifunctional non-viral gene carriers. SCIENCE CHINA Chem. 54, 359–368.
Yin, H., Kanasty, R.L., Eltoukhy, A.A., Vegas, A.J., Dorkin, J.R., Anderson, D.G., 2014. Non-viral vectors for gene-based therapy. Nat. Rev. Genet. 15, 541–555.
Yoeruek, E., Ziemssen, F., Henke-Fahle, S., Tatar, O., Tura, A., Grisanti, S., Bartz-Schmidt, K.U., Szurman, P., Tubingen Bevacizumab Study, G, 2008. Safety, penetration and efficacy of topically applied bevacizumab: evaluation of eyedrops in corneal neovascularization after chemical burn. Acta Ophthalmol. 86, 322–328.
Zhang, S., Gao, H., Bao, G., 2015. Physical Principles of Nanoparticle Cellular Endocytosis. ACS Nano 9, 8655–8671.
Zhao, T., Liang, C., Zhao, Y., Xue, X., Ma, Z., Qi, J., Shen, H., Yang, S., Zhang, J., Jia, Q., Du, Q., Cao, D., Xiang, B., Zhang, H., Qi, X., 2022. Multistage pH-responsive codelivery liposomal platform for synergistic cancer therapy. J. Nanobiotechnol. 20, 177.